

NMR and NQR studies on transition-metal arsenide superconductors $LaRu_2As_2$, $KCa_2Fe_4As_4F_2$, and $A_2Cr_3As_3$

Jun Luo(罗军), Chunguang Wang(王春光), Zhicheng Wang(王志成), Qi Guo(郭琦), Jie Yang(杨杰), Rui Zhou(周睿), K Matano, T Oguchi, Zhian Ren(任治安), Guanghan Cao(曹光旱), Guo-Qing Zheng(郑国庆)

Citation: Chin. Phys. B . 2020, 29(6): 067402 . **doi:** 10.1088/1674-1056/ab892d
Journal homepage: http://cpb.iphy.ac.cn; http://iopscience.iop.org/cpb

What follows is a list of articles you may be interested in

High-magnetic-field induced charge order in high-T_c cuprate superconductors

L X Zheng(郑立玄), J Li(李建), T Wu(吴涛)

Chin. Phys. B . 2019, 28(11): 117402 . **doi:** 10.1088/1674-1056/ab4575

Nuclear magnetic resonance measurement station in SECUF using hybrid superconducting magnets

Zheng Li(李政), Guo-qing Zheng(郑国庆)

Chin. Phys. B . 2018, 27(7): 077404 . **doi:** 10.1088/1674-1056/27/7/077404

Structural phase transition, precursory electronic anomaly, and strong-coupling superconductivity in quasi-skutterudite $(Sr_{1-x}Ca_x)_3Ir_4Sn_{13}$ and $Ca_3Rh_4Sn_{13}$

Jun Luo(罗军), Jie Yang(杨杰), S Maeda, Zheng Li(李政), Guo-Qing Zheng(郑国庆)

Chin. Phys. B . 2018, 27(7): 077401 . **doi:** 10.1088/1674-1056/27/7/077401

Review of nuclear magnetic resonance studies on iron-based superconductors

Ma Long, Yu Wei-Qiang

Chin. Phys. B . 2013, 22(8): 087414 . **doi:** 10.1088/1674-1056/22/8/087414

Quenched Fe moment in the collapsed tetragonal phase of $Ca_{1-x}Pr_xFe_2As_2$

Ma Long, Gi Gao-Feng, Dai Jia, Saha S R, Drye T, Paglione J, Yu Wei-Qiang

Chin. Phys. B . 2013, 22(5): 057401 . **doi:** 10.1088/1674-1056/22/5/057401

NMR and NQR studies on transition-metal arsenide superconductors $LaRu_2As_2$, $KCa_2Fe_4As_4F_2$, and $A_2Cr_3As_3$ *

Jun Luo(罗军)[1,†,‡] Chunguang Wang(王春光)[1,2,†] Zhicheng Wang(王志成)[3], Qi Guo(郭琦)[1], Jie Yang(杨杰)[1], Rui Zhou(周睿)[1,4], K Matano[5], T Oguchi[6], Zhian Ren(任治安)[1,2], Guanghan Cao(曹光旱)[3], and Guo-Qing Zheng(郑国庆)[1,2,5,§]

[1] *Institute of Physics, Chinese Academy of Sciences, and Beijing National Laboratory for Condensed Matter Physics, Beijing* 100190, *China*
[2] *School of Physical Sciences, University of Chinese Academy of Sciences, Beijing* 100049, *China*
[3] *Department of Physics, Zhejiang University, Hangzhou* 310027, *China*
[4] *Songshan Lake Materials Laboratory, Dongguan* 523808, *China*
[5] *Department of Physics, Okayama University, Okayama* 700-8530, *Japan*
[6] *Institute of Scientific and Industrial Research, Osaka University, Osaka* 567-0047, *Japan*

(Received 3 March 2020; revised manuscript received 7 April 2020; accepted manuscript online 15 April 2020)

We report ^{75}As-nuclear magnetic resonance (NMR) and nuclear quadrupole resonance (NQR) measurements on transition-metal arsenides $LaRu_2As_2$, $KCa_2Fe_4As_4F_2$, and $A_2Cr_3As_3$. In the superconducting state of $LaRu_2As_2$, a Hebel–Slichter coherence peak is found in the temperature dependence of the spin-lattice relaxation rate $1/T_1$ just below T_c, which indicates that $LaRu_2As_2$ is a full-gap superperconducor. For $KCa_2Fe_4As_4F_2$, antiferromagnetic spin fluctuations are observed in the normal state. We further find that the anisotropy rate $R_{AF} = T_1^c/T_1^{ab}$ is small and temperature independent, implying that the low energy spin fluctuations are isotropic in spin space. Our results indicate that $KCa_2Fe_4As_4F_2$ is a moderately overdoped iron-arsenide high-temperature superconductor with a stoichiometric composition. For $A_2Cr_3As_3$ (A = Na, K, Rb, Cs), we calculate the electric field gradient by first-principle method and assign the ^{75}As-NQR peaks to two crystallographically different As sites, paving the way for further NMR investigation.

Keywords: transition-metal arsenides, 3d and 4d orbitals, nuclear magnetic resonance, iron-based superconductor

PACS: 74.25.nj, 74.40.–n, 74.25.Dw **DOI:** 10.1088/1674-1056/ab892d

1. Introduction

Transition metal arsenides (TMAs) belong to a big family. The binary TMAs, like TaAs, TaP, NbP, and XP_2 (X = Mo, W),[1] are topological Weyl semimetals, whose low energy excitations in the bulk can be viewed as chiral massless Weyl Fermions. The ternary TMAs show rich novel properties, with examples including density wave[2] and superconductivity.[3] The discovery of superconductivity in transition metal arsenide $LaFeAsO_{1-x}F_x$ opens a door to another high-temperature superconducting family besides cuprates.[4] More importantly, the physical properties of TMAs can be tuned by chemical substitution,[5,6] doping,[4] or pressure.[7] Therefore, transition-metal arsenides provide a rich material base for exploring exotic physical phenomena.

Among the TMA family, compounds with $ThCr_2Si_2$-type layered crystal structure have attracted much attention in condensed matter physics. High temperature superconductivity in AFe_2As_2 (A = Ca, Sr, Ba, etc.) was induced by doping[8] or pressure.[9] Iron and ruthenium are in the same group. Many Ru-based compounds show unconventional superconductivity.[10,11] Naturally, it is practical to look for unconventional superconductivity in ruthenium-based compounds with $ThCr_2Si_2$ structure. Recently, Guo *et al.* found that $LaRu_2As_2$ shows superconductivity with zero resistivity at 6.8 K.[12] $LaRu_2As_2$ and $LaRu_2P_2$ are isostructural and their physical properties have been studied by *ab initio* calculations,[13,14] which indicate that the conduction band electrons are mainly contributed from La-5d and Ru-4d orbitals.

$KCa_2Fe_4As_4F_2$ is a newly discovered superconductor with separated double Fe_2As_2 layers, whose T_c reaches as high as 33.5 K.[15] It can be regarded as the intergrowth of 1111-type CaFeAsF and 122-type KFe_2As_2.[15] The Fe valence in CaFeAsF and KFe_2As_2 is +2 and +2.5, respectively. Appointing the insulted compound CaFeAsF as the parent compound, $KCa_2Fe_4As_4F_2$ can be viewed as a self hole-doping system, which is consistent with the Hall effect measurements and electronic structures calculations.[15,16] In the

*Project supported by the National Natural Science Foundation of China (Grant Nos. 11674377, 11634015, and 11974405), the National Key R&D Program of China (Grant Nos. 2017YFA0302904 and 2016YFA0300502), and J. Y. also acknowledges support by the Youth Innovation Promotion Association of Chinese Academy of Sciences.

†These authors contributed equally.
‡Corresponding author. E-mail: junluo@iphy.ac.cn
§Corresponding author. E-mail: gqzheng123@gmail.com

© 2020 Chinese Physical Society and IOP Publishing Ltd

superconducting state, the inverse square penetration depth (λ_{ab}^{-2}) with a linear temperature dependence detected by muon spin rotation (μSR) suggests a line node in the gap function of $KCa_2Fe_4As_4F_2$ and $CsCa_2Fe_4As_4F_2$.[17,18] However, optical conductivity, thermal conductivity, and ARPES measurements suggest a nodeless gap.[19–21]

$A_2Cr_3As_3$ (A = Na, K, Rb, Cs) is the first chromium-based superconducting family under ambient pressure, with T_c ranging from 8.0 K to 2.2 K.[22–25] In the crystal structure, $[Cr_3As_3]_\infty$ chains are separated by the alkaline metal. Owing to the asymmetric distribution of the alkaline metal, there exists two types of As sites. Density function theory (DFT) calculations show that the Fermi surface is formed by one three-dimensional (3D) band γ and two quasi-one-dimensional (1D) bands α and β.[26,27] Experimental results point to unconventional superconductivity in $A_2Cr_3As_3$.[28–34] In the normal state, ferromagnetic fluctuation (FM) was revealed[29] and further found to be enhanced by small radius alkaline metal replacement.[35] Similar to iron-pnictide superconductors, $A_2Cr_3As_3$ shows a close relationship between magnetic fluctuations and superconductivity. More recently, nontrivial topological aspects in $A_2Cr_3As_3$ have been pointed out.[35,36]

In this work, we perform nuclear magnetic resonance (NMR) and nuclear quadrupole resonance (NQR) measurements on $LaRu_2As_2$, $KCa_2Fe_4As_4F_2$, and $A_2Cr_3As_3$. We investigate the properties of $LaRu_2As_2$ and $KCa_2Fe_4As_4F_2$. For $A_2Cr_3As_3$, we assign the one to one correspondence between the two NQR transition lines and the two As crystallographic sites, by combining with the first-principle calculation.

2. Experiment

Polycrystalline $LaRu_2As_2$ and $KCa_2Fe_4As_4F_2$ samples were grown by conventional solid state reaction, as previously reported in Refs. [12,15]. The single crystals of $A_2Cr_3As_3$ were synthesized by high-temperature solution method with A = Cs, Rb , K, $Na_{0.75}K_{0.25}$ or ion-exchanged reaction with A = Na, the details of synthesis can be found in Refs. [22–25]. The T_c of $LaRu_2As_2$ and $KCa_2Fe_4As_4F_2$ were determined by AC susceptibility using an *in-situ* NMR coil. The electric field gradient (EFG) of $K_2Cr_3As_3$ was calculated by the all electron full-potential linear augmented plane wave (FLAPW) method implemented in Hiroshima Linear-Augmented-Plane-Wave (HiLAPW) code with generalized gradient approximation including spin–orbit coupling.[37] The NMR and NQR spectra were obtained by scanning RF frequency and integrating spin-echo intensity at a fixed magnetic field H_0. The spin-lattice relaxation time T_1 was measured by the saturation-recovery method. The T_1 was obtained by fitting the nuclear magnetization $M(t)$ to $1-M(t)/M_0 = \exp(-3t/T_1)$ in NQR case and $1-M(t)/M_0 = 0.1\exp(-t/T_1)+0.9\exp(-6t/T_1)$ in NMR case, where $M(t)$ and M_0 are the nuclear magnetization at time t after the single comb pulse and at thermal equilibrium, respectively.

3. Results and discussion

3.1. $LaRu_2As_2$

Figure 1 shows the temperature dependence of the resonance frequency of the NMR coil. The superconducting transition temperature T_c of the sample is found to be around 6.2 K, which is similar to an earlier report of $T_c = 6.8$ K determined by DC susceptibility measurement.[12] There are two primitive cells with 10 atoms in one unit cell of $LaRu_2As_2$ as shown in the inset of Fig. 1. The As–Ru–As blocks are intercalated by La atoms, and they are alternately arranged along the c axis. As a result, all As sites are equivalent in $LaRu_2As_2$.

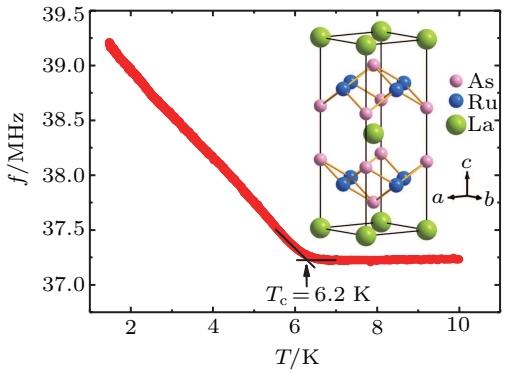


Fig. 1. Temperature dependence of the NMR coil resonance frequency. T_c is determined by the cross point of the two straight lines shown in the figure. The inset shows the crystal structure of $LaRu_2As_2$.

Figure 2(a) shows the ^{75}As NMR spectrum measured at $T = 5$ K under a magnetic field of $\mu_0 H_0 = 12.951$ T, which is a typical powder pattern for nucleus with spin $I = 3/2$. Considering the tetragonal lattice of $LaRu_2As_2$, the total Hamiltonian for $I = 3/2$ nucleus can be expressed as[38]

$$\mathcal{H} = \mathcal{H}_0 + \mathcal{H}_Q = \gamma\hbar I_z H_0(1+K) + \frac{e^2qQ}{4I(2I-1)}[3(I_z^2 - I^2)(3\cos^2\theta - 1)], \quad (1)$$

where K is the Knight shift, $eq = V_{ZZ} = \partial V^2/\partial Z^2$ is the EFG along principle axis Z, Q is the nuclear quadrupole moment, and θ is the angle between the magnetic field and the principle axis of the EFG. The nuclear quadrupole resonance frequency ν_Q is defined as $\frac{3e^2qQ}{2I(2I-1)h}$. The two peaks (marked by two black arrows) observed at 89.2 MHz and 97.8 MHz correspond to the transitions $(3/2 \leftrightarrow 1/2)$ and $(-1/2 \leftrightarrow -3/2)$. The central transition frequency ν_{res} for $I = 3/2$ to the second order is given by[38]

$$\nu_{res} = \gamma H_0(1+K) + \frac{3\nu_Q^2}{16\gamma H_0(1+K)}\sin^2\theta(1-9\cos^2\theta). \quad (2)$$

The observed spectrum is in agreement with the theoretically expected characteristic powder pattern with two peaks at $\theta = 42°$ and $90°$. For a randomly oriented powder sample,

the peak at $\theta = 42°$ would have a larger intensity than that at $\theta = 90°$. Thus our observation suggests that the powder is partially oriented. Figure 2(b) shows the NQR spectrum, in which only one transition ($\pm 1/2 \leftrightarrow \pm 3/2$) is observed, owing to that there is only one As site in this compound. We fitted the ^{75}As NQR spectrum by a Gaussian function, and deduced $\nu_Q = 9.65$ MHz.

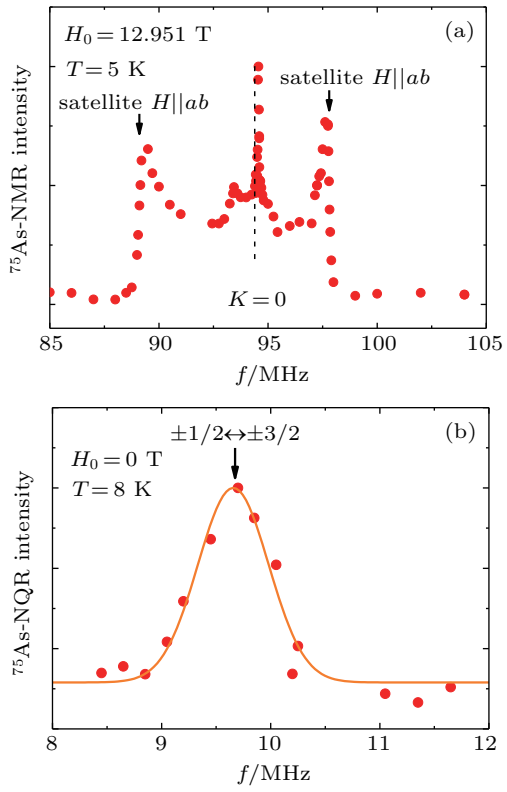


Fig. 2. (a) ^{75}As NMR spectrum of $LaRu_2As_2$ at $T = 5$ K and $H_0 = 12.951$ T. There are two satellite peaks. The central transition frequency ν_{res} has two peaks with $\theta = 42°$ and $\theta = 90°$ due to the second order perturbation. The dashed line corresponds to $K = 0$. (b) ^{75}As NQR spectrum of $LaRu_2As_2$ at $T = 8$ K. The curve is Gaussian fitting of the spectrum.

Figure 3 shows the temperature dependence of $1/T_1$ measured via ^{75}As NQR. The blue dashed line is a guide to the eyes showing the relation of T_1T = constant. We note that $1/T_1$ shows a clear Hebel–Slichter peak just below $T_c = 6.2$ K and decreases exponentially at low temperatures, which are characteristics of an isotropic superconducting gap. The relaxation rate below T_c is expressed as[39]

$$\frac{T_1(T_c)}{T_{1s}} = \frac{2}{k_B T_c} \int N_s(E)^2 \left(1 + \frac{\Delta^2}{E^2}\right) f(E)(1 - f(E))\mathrm{d}E, \quad (3)$$

where Δ is the magnitude of the energy gap, $N_s(E) = N_0 \frac{E}{\sqrt{E^2 - \Delta^2}}$ is the DOS in the superconducting state, $(1 + \Delta^2/E^2)$ is the coherence factor, and $f(E)$ is the Fermi distribution function. We convolute $N_s(E)$ to a rectangular broadening function with a width 2δ and a height $1/2\delta$.[40] The solid curve in Fig. 3 is the simulation with the parameters $2\Delta/k_BT_c = 3.2$ and $r = \Delta/\delta = 12$, which is in good agreement with the experimental data. The value of $2\Delta/k_BT_c$ is close to the BCS value of 3.5.

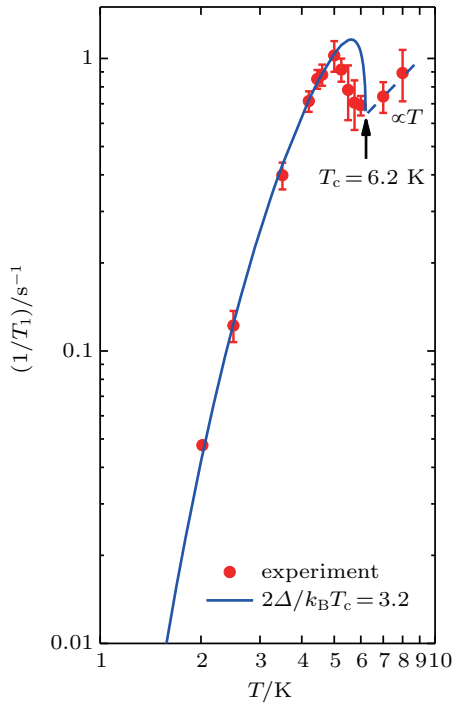


Fig. 3. The temperature dependence of ^{75}As NQR spin-lattice relaxation rate $1/T_1$. $1/T_1$ shows a coherence peak just below T_c. The dashed line shows a T_1T = constant relation. The solid curve is the fitting result assuming an s-wave gap.

3.2. $KCa_2Fe_4As_4F_2$

Figure 4(b) shows a typical NMR spectrum of $KCa_2Fe_4As_4F_2$. There are two types of As sites, as shown in Fig. 4(a), namely, As1 site close to K site and As2 close to Ca site.[15] As mentioned above, there will be two center peaks for each ^{75}As site, with low frequency peak and high frequency peak corresponding to $\theta = 42°$ and $\theta = 90°$, respectively. So the four peaks around the central transition of $KCa_2Fe_4As_4F_2$ are observed, which can be seen more clearly in the inset of Fig. 4(b). We assign the inner two peaks to the As1 site and outer two peaks to the As2 site, as will be elaborated below.

Figure 4(c) shows the waterfall plot of NQR spectrums of As2 site at different temperatures. No splitting or broadening is seen in the NQR spectrums, indicating that magnetic order is absent in the studied compound. By using a Lorentz function to fit the spectrums, we deduced the temperature dependence of ν_Q, as summarized in Fig. 5(a). The ν_Q of the As2 site increases from $T = 275$ K to 50 K but saturates below 50 K, as also seen in the As2 site of $CaKFe_4As_4$.[41] The $\nu_Q(100\ \mathrm{K})$ of the As1 site is 10.9 MHz and $\nu_Q(130\ \mathrm{K})$ of the As2 site is 20.1 MHz, close to $\nu_Q(100\ \mathrm{K}) = 12.4$ MHz of KFe_2As_2[42] and $\nu_Q(130\ \mathrm{K}) = 19.2$ MHz of CaFeAsF.[43] We therefore assign the inner two peaks of the central peaks to the As1 site and the outer two peaks of the central peaks to the As2 site.

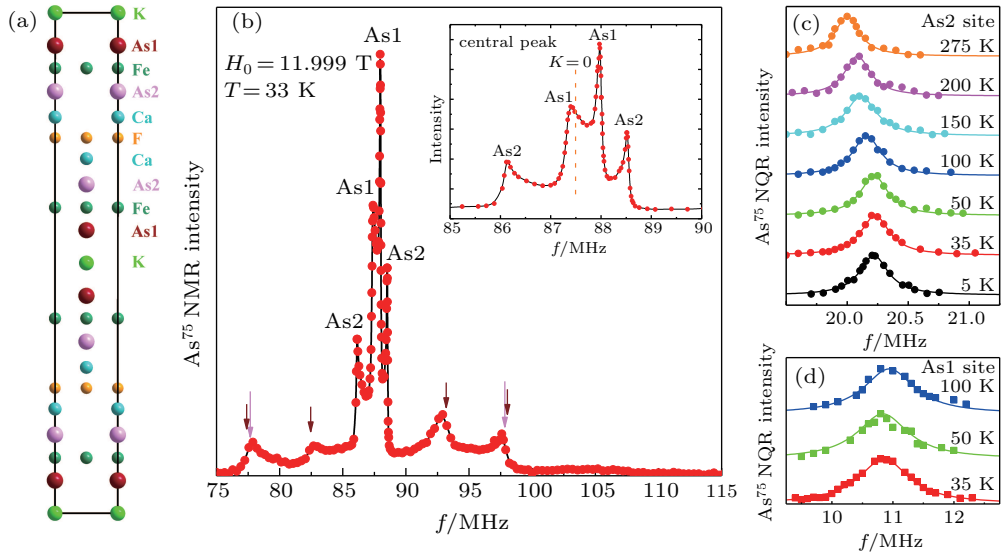


Fig. 4. (a) Crystal structure of $KCa_2Fe_4As_4F_2$. There are two types of As sites marked by dark red and pink, respectively. (b) Nuclear magnetic resonance spectrum of $KCa_2Fe_4As_4F_2$ at $H_0 = 11.999$ T and $T = 33$ K. The dark red arrow and pink arrow correspond to the satellite peaks of As1 site and As2 site, respectively. Insets: central peaks after zooming in. Temperature dependence of NQR spectrums of (c) As2 site and (d) As1 site.

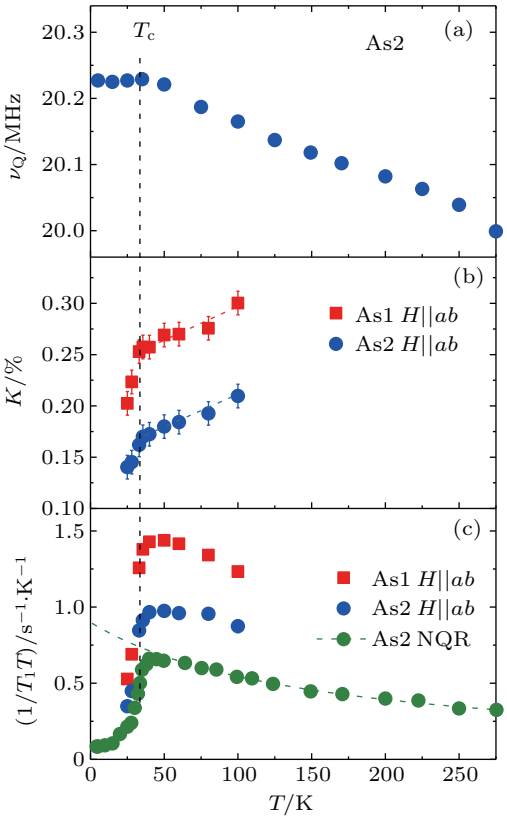


Fig. 5. (a) Temperature dependence of ν_Q of the As2 site. (b) Temperature dependence of Knight shift for the two As sites. (c) Temperature dependence of $1/T_1T$ measured at the two NMR peaks corresponding to $\theta = 90°$ at $H = 11.999$ T and As2 site at $H = 0$ T. The olive dashed curve is a fitting by the 2D antiferromagnetic fluctuations model. The black dashed-dotted line characterizes T_c.

After subtracting the second order perturbation effect according to Eq. (2), the Knight shift for As1 site and As2 site, is obtained as shown in Fig. 5(b). The Knight shift decreases from $T = 100$ K to T_c, which is similar to most of iron based superconductors.[44–48] The spin-lattice relaxation rate $1/T_1$ was measured at two central peaks corresponding to $\theta = 90°$ which has a stronger intensity, and also at NQR peak of As2 sites. The results are presented in Fig. 5(c). The magnitude of both K and $1/T_1T$ for As1 site is bigger than that of As2 site. This is likely due to different hyperfine coupling constants at the two sites. In iron-based superconductors, hyperfine coupling is determined by the overlap of the electron cloud between Fe and As, namely, by the distance between Fe and As. From the original data in Ref. [15], we obtain the distances between As and Fe planes h(As-Fe) to be 1.405 Å and 1.436 Å for As1 site and As2 site, respectively. A smaller h(As1-Fe) leads to a bigger hyperfine coupling constant, which can explain the larger K and $1/T_1T$ for As1 site. The difference in the magnitude between $1/T_1T$ obtained by NMR and NQR will be explained later. The $1/T_1T$ shows a monotonic increase as the temperature decreases from $T = 275$ K to 40 K, indicating the existence of antiferromagnetic spin fluctuations in $KCa_2Fe_4As_4F_2$. We use a phenomenological 2D antiferromagnetic fluctuations model[49,50] $1/T_1T \propto a + C/(T + \Theta)$ to fit our data, where $C/(T + \Theta)$ is related to the low energy spin fluctuations and a is due to other contributions. The fitting result is shown by the olive dashed curve in Fig. 5(c). We obtain $a = 0.015$ s^{-1}·K^{-1} and $\Theta = 149$ K. Figure 6 shows the comparison of $1/T_1T$ between $KCa_2Fe_4As_4F_2$ and $Ba_{0.45}K_{0.55}Fe_2As_2$. After shifting the starting point of the right axis upward by 0.32 s^{-1}·K^{-1}, we see that the $1/T_1T$ of these two compounds are scaled very well. Thus it seems that the low energy spin fluctuations are quite similar for these two compounds. As seen in Fig. 6, the dynamic susceptibility starts to decrease at $T \approx 40$ K (above T_c), which is qualitatively similar to the features observed in cuperates.[51] This 'pseudogap' behavior was also observed in $Ba_{0.45}K_{0.55}Fe_2As_2$[52] and over-doped La1111.[53,54] The valence of Fe in $KCa_2Fe_4As_4F_2$ is +2.25, meaning that the

equivalent doping level is 0.25 hole/Fe. This is close to the value in $Ba_{0.45}K_{0.55}Fe_2As_2$, where the doping level is 0.275 hole/Fe.

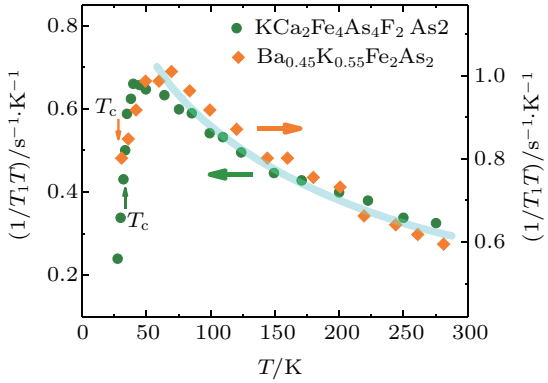


Fig. 6. Comparison of $1/T_1T$ for $KCa_2Fe_4As_4F_2$ and $Ba_{0.45}K_{0.55}Fe_2As_2$. For clarity, the starting point of the right axis is 0.32 $s^{-1}\cdot K^{-1}$ higher than that of the left axis. The scale of the two axes is the same.

To further study the nature of the AFM spin fluctuations, we compare the $1/T_1$ for H_0 parallel to c direction and perpendicular to c direction. In this compound, the principle axis of EFG is along c direction. Therefore, T_1 measured in the NMR central peaks with $\theta = 90^\circ$ corresponds to T_1^{ab}, while T_1 measured in the NQR peaks corresponds to T_1^c, as the principle axis of EFG is along the c direction. Then we can obtain the anisotropy ratio of $1/T_1T$, $R_{\rm AF} = T_1^c/T_1^{ab}$. We find that it is only around 1.5 and nearly temperature-independent as shown in Fig. 7. For the stripe order where the wave vectors of the spin fluctuations are $[\pi, 0]$ and $[0, \pi]$,[45,55] $1/T_1^{ab}$ and $1/T_1^c$ can be expressed as

$$1/T_1^{ab} \propto A^2[\chi_a''(\omega_0,Q)+\chi_b''(\omega_0,Q)+\chi_c''(\omega_0,Q)]/2, \quad (4)$$

$$1/T_1^{c} \propto A^2\chi_c''(\omega_0,Q), \quad (5)$$

where A is the hyperfine coupling constant and $\chi_i''(\omega_0,Q)$ is the imaginary part of the dynamic susceptibility along i ($i = a$, b, c) direction at the measured angular frequency ω_0. Therefore, one obtains

$$R_{\rm AF} = \frac{\chi_a''(\omega_0,Q)+\chi_b''(\omega_0,Q)}{2\chi_c''(\omega_0,Q)} + \frac{1}{2}. \quad (6)$$

If $\chi_a''(\omega_0,Q) = \chi_b''(\omega_0,Q) = \chi_c''(\omega_0,Q)$, the ratio $R_{\rm AF}$ will be equal to 1.5. Thus our observation suggests that the low energy spin fluctuations are isotropic in spin space. This is in sharp contrast with the spin fluctuations of the optimally-doped $Ba_{0.68}K_{0.32}Fe_2As_2$, which are anisotropic.[45] This result again indicates that the origin of the low energy spin fluctuations in $KCa_2Fe_4As_4F_2$ is different from that in the optimally-doped $Ba_{0.68}K_{0.32}Fe_2As_2$. The anisotropic spin fluctuations in $Ba_{0.68}K_{0.32}Fe_2As_2$ were ascribed to a spin–orbit coupling (SOC) which was estimated to be 10–20 meV. Our result therefore suggests that the SOC is smaller in $KCa_2Fe_4As_4F_2$. Rather, the stoichiometric compound $KCa_2Fe_4As_4F_2$ provides a unique platform for studying the overdoped region of iron-based superconductors. Equations (4) and (5) also explain why $1/T_1T$ obtained by NQR is smaller than that by NMR, as in the former case the quantized axis is along the c-axis.

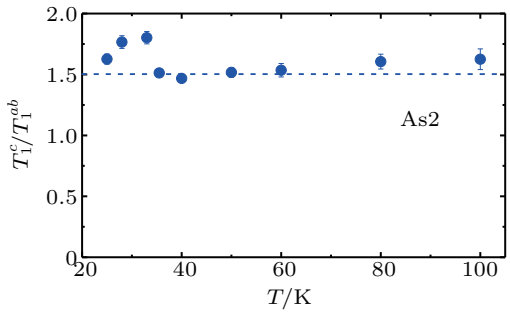


Fig. 7. Temperature dependence of the ratio T_1^c/T_1^{ab} for As2 sites.

Finally, we discuss the property in the superconducting state. Figure 8 shows the temperature dependence of $1/T_1$. Below T_c, no coherence peak appears and T_1 decreases more rapidly than T^3. Below $T = 15$ K, $1/T_1$ starts to be proportional to T, indicating the existence of strong impurity scattering in this sample.[56,57] We further simulate our results by assuming different gap symmetries as shown in Fig. 8. In the past decade of researches on iron-pnictides, multiple gaps have been found.[58–60] In fact, the s^{+-} wave gap symmetry in which the gap sign reverses between hole Fermi pocket and electron Fermi pocket can account for the hump behavior of $1/T_1$ in various compounds.[44,45,53] Due to strong impurity scattering, however, the hump feature in $1/T_1$ is not visible in the present case. We tried to fit our data with various models. A simple d-wave model with $\Delta^{\rm d} = 2.5k_{\rm B}T_c$ or a two-band (two gap) s^{+-} wave with $\Delta_1^{\rm s} = 2k_{\rm B}T_c$, $\Delta_2^{\rm s} = 3.75k_{\rm B}T_c$ and equal weight for the two bands deviates from our data severely at low temperatures. Following the T_1 calculation method of d-wave with impurity in literature,[57] we found that the parameter $\Delta^{\rm d} = 2.5k_{\rm B}T_c$, $\eta = 0.064\Delta^{\rm d}$ can fit our data well. On the other hand, two-gap s^{+-}-wave with impurity scattering can also account for our data. In the s^{+-}-wave model,[61] $1/T_1$ is expressed as

$$\frac{1}{T_1} \sim -T\int_0^\infty {\rm d}\omega \frac{\partial f(\omega)}{\partial \omega}(W_{\rm GG}+W_{\rm FF}), \quad (7)$$

$$W_{\rm GG} = \left[\sum_{a={\rm h,e}} N_a(0)\left\langle {\rm Re}\frac{\omega}{\sqrt{\omega^2-\Delta_a^2(k)}}\right\rangle_k\right]^2, \quad (8)$$

$$W_{\rm FF} = \left[\sum_{a={\rm h,e}} N_a(0)\left\langle {\rm Re}\frac{\Delta_a(k)}{\sqrt{\omega^2-\Delta_a^2(k)}}\right\rangle_k\right]^2, \quad (9)$$

where N_a is DOS in hole or electron Fermi surface. We define $\alpha = \frac{N_{\rm e}}{N_{\rm e}+N_{\rm h}}$. If there exists impurity scattering, ω will be replaced by $\omega + i\eta$. Using this model, we found that the parameters $\Delta_1^{\rm s} = 2k_{\rm B}T_c$, $\Delta_2^{\rm s} = 3.75k_{\rm B}T_c$, $\alpha = 0.5$, $\eta = 0.21\Delta_1^{\rm s}$ reproduce our data well. In order to distinguish d-wave and s^{+-}-wave, more measurements on a single crystal are required.

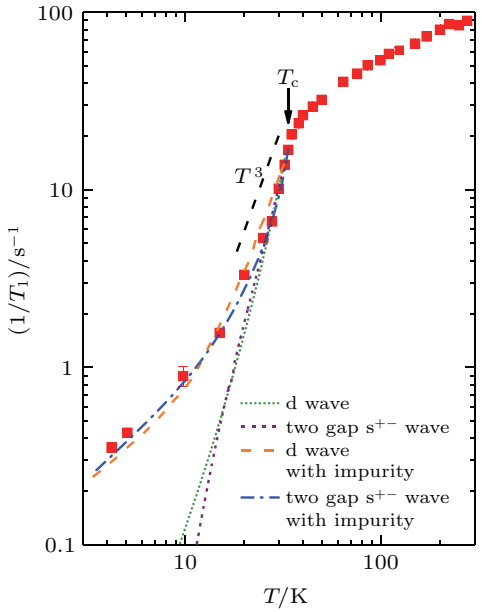


Fig. 8. Temperature dependence of $1/T_1$ in $KCa_2Fe_4As_4F_2$. The black dashed line is a guide to the eyes, indicating a T^3 variation of $1/T_1$. The green dotted, purple short-dashed, blue dashed-dotted, and orange dashed curves show the fitting results of d wave, two-gap s^{+-} wave, d wave with impurity scattering, and two-gap s^{+-} wave with impurity scattering, respectively.

3.3. $A_2Cr_3As_3$

Next, we turn to $A_2Cr_3As_3$ (A = Na, $Na_{0.75}K_{0.25}$, K, Rb, Cs). Figure 9(a) shows the NQR spectra for $A_2Cr_3As_3$ at T = 150 K, the five samples commonly show two peaks originating from two inequivalent As sites. In the previous reports, the site assignment was not performed. We assign the left peak to As2 site and the other peak to As1 site based on the following two facts. Firstly, neutron diffraction measurements found a displacement of the K2 sites towards CrAs tube with decreasing temperature in $K_2Cr_3As_3$.[62] As shown in Fig. 9(b), the As1 site has four nearest A1 neighbors, while the As2 has two nearest A1 neighbors and two nearest A2 neighbors. Therefore, the displacement of the A2 sites makes a stronger variation of the EFG for the As2 sites, leading to a stronger temperature variation of ν_Q for As2 site than As1 site. Indeed, the change of ν_Q defined as $\delta\nu_Q = \delta\nu_Q(T = 4.2\ \text{K}) - \delta\nu_Q(T = 300\ \text{K})$ is bigger for the left peak than that for the right peak.[28,29,63] It can be seen more clearly in Fig. 9(c), where we normalize the original ν_Q data by $\nu_Q(T = 4.2\ \text{K})$. Secondly, we calculate the EFG of two As sites for $K_2Cr_3As_3$. The calculation is based on HiLAPW which is an extension of FLAPW.[37] We use generalized-gradient approximation (GGA) as the exchange correlation function, and include SOC. The nuclear quadrupole moment $Q = 3.141 \times 10^{-29}$ m^2 was used for nucleus ^{75}As.[64] The inputting lattice constant is from Ref. [22] at T = 300 K. The calculational result is shown in Table 1. The EFG tensors are defined as $V_{\alpha\alpha} = \partial V^2/\partial\alpha^2$ ($\alpha = X, Y, Z$), where V is the electric potential. In case of $\eta = \frac{V_{XX}-V_{YY}}{V_{ZZ}} \neq 0$, the ν_Q is defined as $\frac{3e^2qQ\sqrt{1+\eta^2/3}}{2I(2I-1)h}$, where EFG $eq = V_{ZZ}$ and V_{ZZ} is the principle-axis value. As shown in Fig. 10, the principle axis of $A_2Cr_3As_3$ is in the ab plane. The resulting ν_Q = 41.64 MHz of As1 site is bigger than ν_Q = 39.94 MHz of As2 site, which supports the above mentioned site assignment. The site assignment will help further study the physical properties of two As sites by NMR, which is vitally important to identify the pairing symmetry.

Table 1. Comparison of experimental and theoretical results of ν_Q for $K_2Cr_3As_3$. The experimental data were obtained at 300 K. In the EFG calculation, the lattice constant at 300 K which was referred from Ref. [22] was used. The units of $V_{\alpha\alpha} = \partial V^2/\partial\alpha^2$ ($\alpha = X, Y, Z$) and ν_Q are 10^{19} V/m^2 and MHz, respectively.

Site	V_{XX}	V_{YY}	V_{ZZ}	ν_Q	ν_Q(exp)
As1	–526.35	–570.91	1097.27	41.64	43.6
As2	–524.51	–528.48	1052.98	39.94	38.4

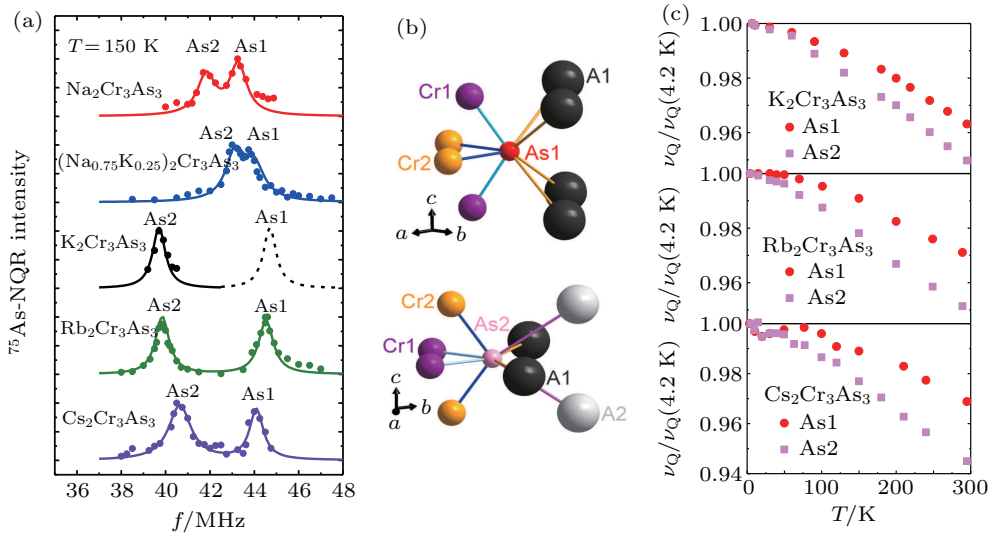


Fig. 9. (a) ^{75}As NQR spectra of $A_2Cr_3As_3$ (A = Na, $Na_{0.75}K_{0.25}$, K, Rb, Cs) measured at T = 150 K. The two peaks correspond to two As sites, namely, As1 site and As2 site. The data for the right peak of $K_2Cr_3As_3$ was referred from Ref. [28]. (b) Surrounding environments of As1 site and As2 site, respectively. (c) Temperature dependence of ν_Q normalized by its value at 4.2 K. The original data of $K_2Cr_3As_3$ and $Cs_2Cr_3As_3$ were referred from Refs. [28,63].

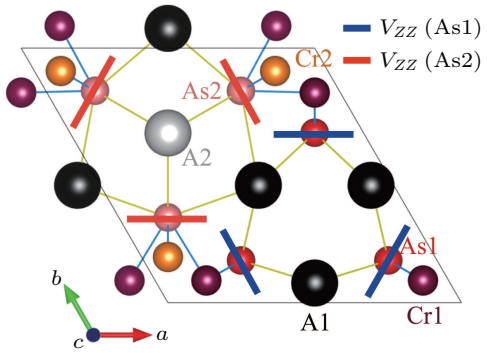


Fig. 10. EFG principle axes (V_{ZZ}) for $K_2Cr_3As_3$, which are shown by the blue and red sticks for As1 site and As2 site, respectively.

Before closing, we note that the three transition-metal arsenides reported here show quite different normal-state properties and the superconducting gap symmetry in these compounds is also different. $LaRu_2As_2$ shows superconductivity with a full gap, whose origin maybe electron–phonon coupling.[13,14] On the other hand, unconventional superconductivity is caused by AFM spin fluctuations in $KCa_2Fe_4As_4F_2$ and FM spin fluctuation in $A_2Cr_3As_3$.[29,35] Future issues include clarifying whether spin triplet pairing is realized by the FM spin fluctuation in $A_2Cr_3As_3$.

4. Conclusion

We have performed NMR and NQR measurements on three types of transition metal arsenides, $LaRu_2As_2$, $KCa_2Fe_4As_4F_2$, and $A_2Cr_3As_3$. In $LaRu_2As_2$, different from Fe-based superconductors with the same crystal structure, a coherence peak in the temperature dependence of $1/T_1$ appears just below T_c, indicating that the superconducting gap is fully open. In double Fe_2As_2 layers compound $KCa_2Fe_4As_4F_2$, the strength of antiferromagnetic spin fluctuations is found to be similar to that in $Ba_{0.45}K_{0.55}Fe_2As_2$, indicating that the stoichiometric compound $KCa_2Fe_4As_4F_2$ is in the moderately hole-overdoped region. In fact, the anisotropy of $1/T_1$, $R_{AF} = T_1^c/T_1^{ab}$ is only 1.5, implying that the spin fluctuations are isotropic, which is in sharp contrast to the nearly optimally-doped $Ba_{0.68}K_{0.32}Fe_2As_2$. For $A_2Cr_3As_3$, we identified the one-to-one correspondence between NQR peaks and As sites. Our research revealed a wide variety of the physical properties of transition metal arsenides.

Acknowledgement

We thank Y. G. Shi, C. J. Yi, Q. G. Mu, Z. T. Tang, and T. Liu for early collaborations.

References

[1] Weng H, Fang C, Fang Z, Bernevig B A and Dai X 2015 *Phys. Rev. X* **5** 011029
[2] Rotter M, Tegel M, Johrendt D, Schellenberg I, Hermes W and Pöttgen R 2008 *Phy. Rev. B* **78** 020503
[3] Jeitschko W, Glaum R and Boonk L 1987 *J. Solid State Chem.* **69** 93
[4] Kamihara Y, Watanabe T, Hirano M and Hosono H 2008 *J. Am. Chem. Soc.* **130** 3296
[5] Eilers F, Grube K, Zocco D A, Wolf T, Merz M, Schweiss P, Heid R, Eder R, Yu R, Zhu J X, Si Q M, Shibauchi T and Löhneysen H V 2016 *Phys. Rev. Lett.* **116** 237003
[6] Wu Y P, Zhao D, Wang A F, Wang N Z, Xiang Z J, Luo X G, Wu T and Chen X H 2016 *Phys. Rev. Lett.* **116** 147001
[7] Wu W, Cheng J G, Matsubayashi K, Kong P P, Lin F K, Jin C Q, Wang N L, Uwatoko Y and Luo J L 2014 *Nat. Commun.* **5** 5508
[8] Rotter M, Tegel M and Johrendt D 2008 *Phys. Rev. Lett.* **101** 107006
[9] Alireza P L, Ko Y T, Gillett J, Petrone C M, Cole J M, Lonzarich G G and Sebastian S E 2009 *J. Phys. Condens. Matter* **21** 012208
[10] Maeno Y, Hashimoto H, Yoshida K, Nishizaki S, Fujita T, Bednorz J G and Lichtenberg F 1994 *Nature* (London) **372** 532
[11] Palstra T T, Menovsky A A, van den Berg J, Dirkmaat A J, Kes P H, Nieuwenhuys G J and Mydosh J A 1985 *Phys. Rev. Lett.* **55** 2727
[12] Guo Q, Pan B J, Yu J, Ruan B B, Chen D Y, Wang X C, Mu Q G, Chen G F and Ren Z A 2016 *Sci. Bull.* **61** 921
[13] Hadi M A , Ali M S, Naqib S H and Islam A K M A 2017 *Chin. Phys. B* **26** 037103
[14] Rahaman M Z and Rahman M A 2017 *Journal of Alloys and Compounds* **695** 2827
[15] Wang Z C, He C Y, Wu S Q, Tang Z T, Liu Y, Ablimit A, Feng C M and Cao G H 2016 *J. Am. Chem. Soc.* **138** 7856
[16] Wang G T, Wang Z W and Shi X B 2016 *Euro. Phys. Lett.* **116** 37003
[17] Kirschner F K K, Adroja D T, Wang Z C, Lang F, Smidman M, Baker P J, Cao G H and Blundell S J 2018 *Phys. Rev. B* **97** 060506(R)
[18] Smidman M, Kirschner F K K, Adroja D T, Hillier A D, Lang F, Wang Z C, Cao G H and Blundell S J 2018 *Phys. Rev. B* **97** 060509(R)
[19] Xu B, Wang Z C, Sheveleva E, Lyzwa F, Marsik P, Cao G H and Bernhard C 2019 *Phys. Rev. B* **99** 125119
[20] Huang Y Y, Wang Z C, Yu Y J, Ni J M, Li Q, Cheng E J, Cao G H and Li S Y 2019 *Phys. Rev. B* **99** 020502(R)
[21] Wu D S, Hong W S, Dong C X, Wu X X, Sui Q T, Huang J W, Gao Q, Li C, Song C Y, Luo H L, Yin C H, Xu Y, Luo X Y, Cai Y Q, Jia J J, Wang Q Y, Huang Y, Liu G D, Zhang S J, Zhang F F, Yang F, Wang Z M, Peng Q J, Xu Z Y, Qiu X G, Li S L, Luo H Q, Hu J P, Zhao L and Zhou X J 2020 arXiv:2001.04082v1
[22] Bao J K, Liu J Y, Ma C W, Meng Z H, Tang Z T, Sun Y L, Zhai H F, Jiang H, Bai H, Feng C M, Xu Z A and Cao G H 2015 *Phys. Rev. X* **5** 011013
[23] Tang Z T, Bao J K, Liu Y, Sun Y L, Ablimit A, Zhai H F, Jiang H, Feng C M, Xu Z A and Cao G H 2015 *Phys. Rev. B* **91** 020506(R)
[24] Tang Z T, Bao J K, Wang Z, Bai H, Jiang H, Liu Y, Zhai H F, Feng C M, Xu Z A and Cao G H 2015 *Sci. China Mater.* **58** 16
[25] Mu Q G, Ruan B B, Pan B J, Liu T, Yu J, Zhao K, Chen G F and Ren Z A 2018 *Phys. Rev. Materials* **2** 034803
[26] Jiang H, Cao G H and Cao C 2015 *Sci. Rep.* **5** 16054
[27] Wu X X, Le C C, Yuan J, Fan H and Hu J P 2015 *Chin. Phys. Lett.* **5** 057401
[28] Zhi H Z, Imai T, Ning F L, Bao J K and Cao G H 2015 *Phys. Rev. Lett.* **114** 147004
[29] Yang J, Tang Z T, Cao G H and Zheng G Q 2015 *Phys. Rev. Lett.* **115** 147002
[30] Pang G M, Smidman M, Jiang W B, Bao J K, Weng Z F, Wang Y F, Jiao L, Zhang J L, Cao G H and Yuan H Q 2015 *Phys. Rev. B* **91** 220502
[31] Adroja D T, Bhattacharyya A, Telling M, Feng Y, Smidman M, Pan B, Zhao J, Hillier A D, Pratt F L and Strydom A M 2015 *Phys. Rev. B* **92** 134550
[32] Adroja D T, Bhattacharyya A, Smidman M, Hillier A, Feng Y, Pan B, Zhao J, Lees M R, Strydom A and Biswas P K 2017 *J. Phys. Soc. Jpn.* **86** 044710
[33] Zuo H, Bao J K, Liu Y, Wang J, Jin Z, Xia Z, Li L, Xu Z, Kang J, Zhu Z and Cao G H 2017 *Phys. Rev. B* **95** 014502
[34] Shao Y T, Wu X X, Wang L, Shi Y G, Hu J P and Luo J L 2018 *Euro. Phys. Lett.* **123** 57001
[35] Luo J, Yang J, Zhou R, Mu Q G, Liu T, Ren Z A, Yi C J, Shi Y G and Zheng G Q 2019 *Phys. Rev. Lett.* **123** 047001
[36] Liu C C, Lu C, Zhang L D, Wu X, Fang C and Yang F 2019 arXiv:1909.00943v1
[37] Oguchi T 2001 *Phys. Rev. B* **63** 125115
[38] Abragam A 1961 *The Principles of Nuclear Magnetism* (London: Oxford University Press)
[39] Maclaughlin D E 1976 *Solid State Phys.* **31** 1

[40] Hebel L C 1959 *Phys. Rev.* **116** 79
[41] Cui J, Ding Q P, Meier W R, Böhmer A E, Kong T, Borisov V, Lee Y, Bud'ko S L, Valentí R, Canfield P C and Furukawa Y 2017 *Phys. Rev. B* **96** 104512
[42] Wiecki P, Taufour V, Chung D Y, Kanatzidis M G, Bud'ko S L, Canfield P C and Furukawa Y 2018 *Phys. Rev. B* **97** 064509
[43] Fujiwara N, Matsuishi S, Kamihara Y and Hosono H 2013 *J. Supercond. Nov. Magn.* **26** 2689
[44] Li Z, Ooe Y, Wang X C, Liu Q Q, Jin C Q, Ichioka M and Zheng G Q 2010 *J. Phys. Soc. Jpn.* **79** 083702
[45] Li Z, Sun D L, Lin C T, Su Y H, Hu J P and Zheng G Q 2011 *Phys. Rev. B* **83** 140506(R)
[46] Zhou R, Li Z, Yang J, Sun D L, Lin C T and Zheng G Q 2013 *Nat. Commun.* **4** 2265
[47] Yang J, Zhou R, Wei L L, Yang H X, Li J Q, Zhao Z X and Zheng G Q 2015 *Chin. Phys. Lett.* **32** 107401
[48] Wang C G, Li Z, Yang J, Xing L Y, Dai G Y, Wang X C, Jin C Q, Zhou R and Zheng G Q 2018 *Phys. Rev. Lett.* **121** 167004
[49] Moriya T 1963 *J. Phys. Soc. Jpn.* **18** 516
[50] Moriya T 1985 *Spin Fluctuations in Itinerant Electron Magnetism* (Berlin: Springer-Verlag)
[51] Alloul H, Ohno T and Mendels P 1989 *Phys. Rev. Lett.* **63** 1700
[52] Hirano M, Yamada Y, Saito T, Nagashima R, Konishi T, Toriyama T, Ohta Y, Fukazawa H, Kohori Y, Furukawa Y, Kihou K, Lee C H, Iyo A and Eisaki H 2012 *J. Phys. Soc. Jpn.* **81** 054704
[53] Oka T, Li Z, Kawasaki S, Chen G F, Wang N L and Zheng G Q 2012 *Phys. Rev. Lett.* **108** 047001
[54] Yang J, Oka T, Li Z, Yang H X, Li J Q, Chen G F and Zheng G Q 2018 *Science China Physics, Mechanics & Astronomy* **61** 117411
[55] Kitagawa K, Katayama N, Ohgushi K, Yoshida M and Takigawa M 2008 *J. Phys. Soc. Jpn.* **77** 114709
[56] Asayama K, Zheng G Q, Kitaoka Y, Ishida K and Fujiwara K 1991 *Physica C* **178** 281
[57] Bang Y K, Graf M J, Balatsky A V and Thompson J D 2004 *Phys. Rev. B* **69** 014505
[58] Matano K, Ren Z A, Dong X L, Sun L L, Zhao Z X and Zheng G Q 2008 *Euro. Phys. Lett.* **83** 57001
[59] Kawasaki S, Shimada K, Chen G F, Luo J L, Wang N L and Zheng G Q 2008 *Phys. Rev. B* **78** 220506
[60] Wang Z C, Liu Y, Wu S Q, Shao Y T, Ren Z and Cao G H 2019 *Phys. Rev. B* **99** 144501
[61] Bang Y K and Choi H Y 2008 *Phys. Rev. B* **78** 134523
[62] Taddei K M, Xing G Z, Sun J F, Fu Y H, Li Y W, Zheng Q, Sefat A S, Singh D J and Cruz C de la 2018 *Phys. Rev. Lett.* **121** 187002
[63] Zhi H Z, Lee D, Imai T, Tang Z T, Liu Y and Cao G H 2016 *Phys. Rev. B* **93** 174508
[64] Effenberger B, Kunold W, Oesterle W, Schneider M, Simons L M, Abela R and Wüest J 1982 *Z. Phys.* **A309** 77